Geophysical Research Letters

Supporting Information for

An anisotropic contrast in the lithosphere across the central San Andreas fault

Chengxin Jiang[1], Brandon Schmandt[1], Robert W. Clayton[2]

[1] Department of Earth and Planetary Sciences, University of New Mexico, Albuquerque, NM 87131.

[2] Seismological Laboratory, California Institute of Technology, Caltech 252-21, Pasadena, CA 91125.

Contents of this file

Introduction

This supporting file contains the following figures and table:

Figure S1. An example of selected non-null splitting measurement for a SKS arrival at station CC17.
Figure S2. Quality control criteria for each parameter used for the selection of good null and non-null measurements in this study.
Figure S3. Compilations of splitting results from using a different culling threshold of defining the null measurements.
Figure S4. Comparison of splitting parameters and associated uncertainties from using a different culling threshold of SNR with the same criteria of 10° angular difference between fast direction and event back-azimuth to define null measurements.
Figure S5: Comparison of splitting parameters and associated uncertainties from using a different culling threshold of SNR with the same criteria of 15° angular difference between fast direction and event back-azimuth to define null measurements.
Figure S6: Rose diagrams showing the fast direction of each non-null station.
Figure S7: Comparison of the splitting fast direction at SAFOD sites with those from our study.
Figure S8: Synthetic splitting results for modelling observed azimuth-dependent splitting behaviors for stations located within 30 km on both sides of the SAF.
Table S1: Definitions of the parameter used for the quality control in section 2.
Table S2: Summary of the stacked SKS/SKKS splitting measurements along CCSE array as well as for 7 long-term regional stations.

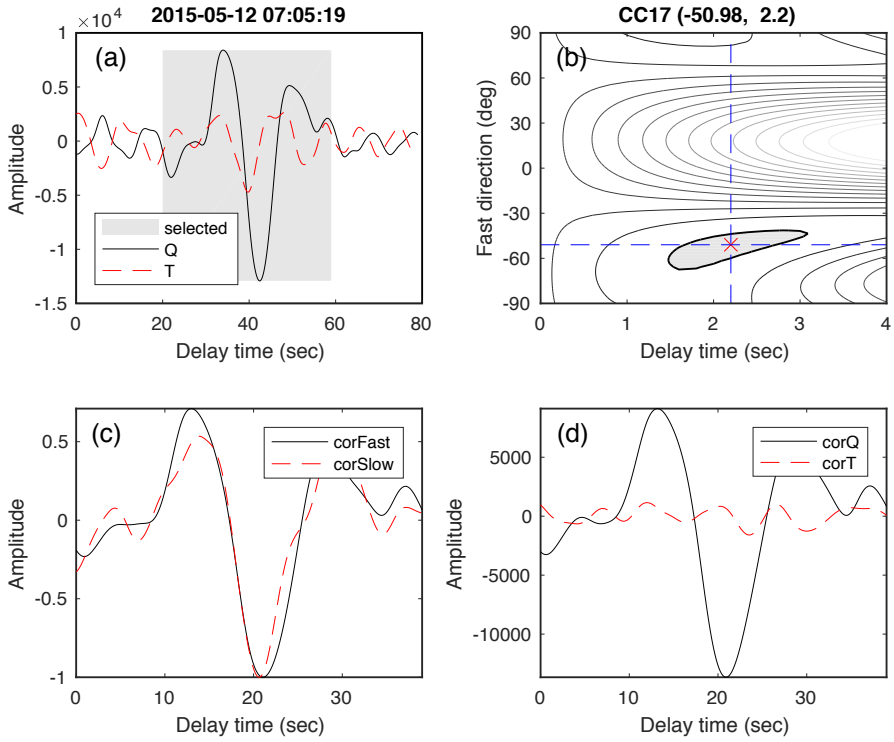

Figure S1. An example of selected non-null splitting measurement for a SKS arrival at station CC17. (a) The raw radial (solid black line) and transverse (dashed red line) waveform components. The grey corridor shows the selected time window for subsequent splitting analysis. (b) Diagnostic plot resulted from the grid-search based splitting analysis with the x-axis showing the delay time and the y axis showing the fast direction. The grey shaded region represents the estimates of 95% confidence, and the red cross denotes the optimal splitting parameters with exact values marked on the top of the figure. (c) Corrected waveforms for the fast (solid black line) and slow direction (dashed red line). (d) Corrected Q (solid black line) and T (dashed red line) waveforms.

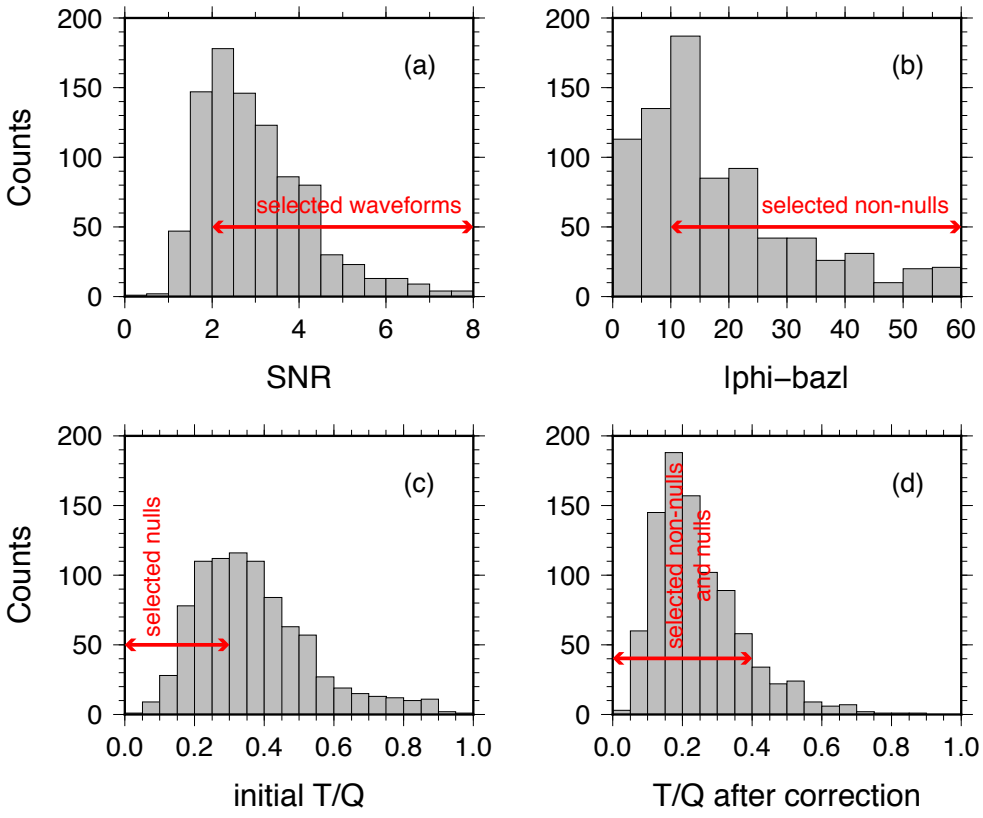

Figure S2. Quality control criteria for each parameter (defined in Table S1) used for the selection of good null and non-null measurements in this study, including SNR (a), angular difference (b), T-to-Q amplitude ratio of raw waveforms (c), and T-to-Q amplitude ratio for corrected waveforms (d). The red lines with arrows denote the range of each parameter to define good non-null and null measurements.

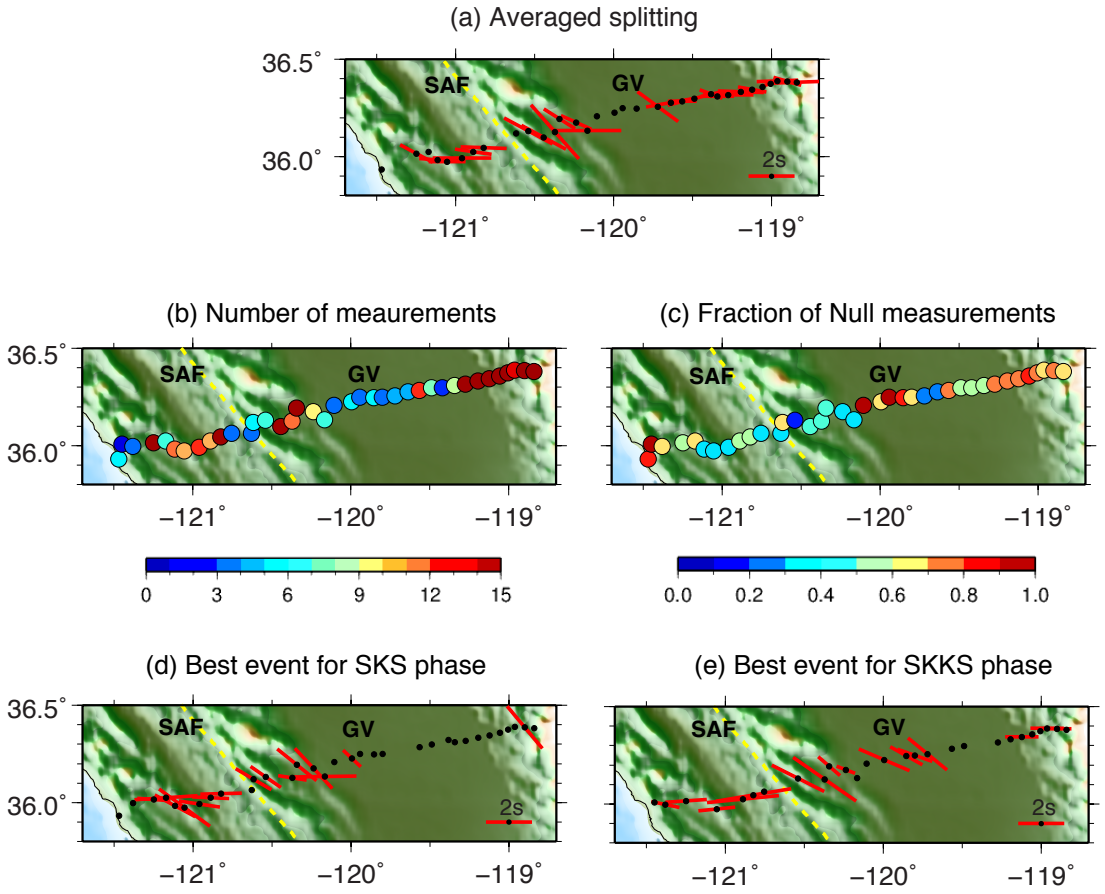

Figure S3. Compilations of splitting results from using a different culling threshold, which requires non-null measurements to have angular differences between fast direction and backazimuth direction larger than 15° (compared to an original culling threshold of 10°). (a) The averaged splitting parameter for the CCSE array resulted from the new data culling; (b) number of measurements at each CCSE stations; (c) fraction of null measurements for each station; (d) the splitting measurements for the best SKS event; (e) the splitting measurements for the best SKKS event. Note the results here are similar to those in Figure 2 and Figure 3a. Abbreviations: SAF-San Andreas Fault, GV-Great Valley.

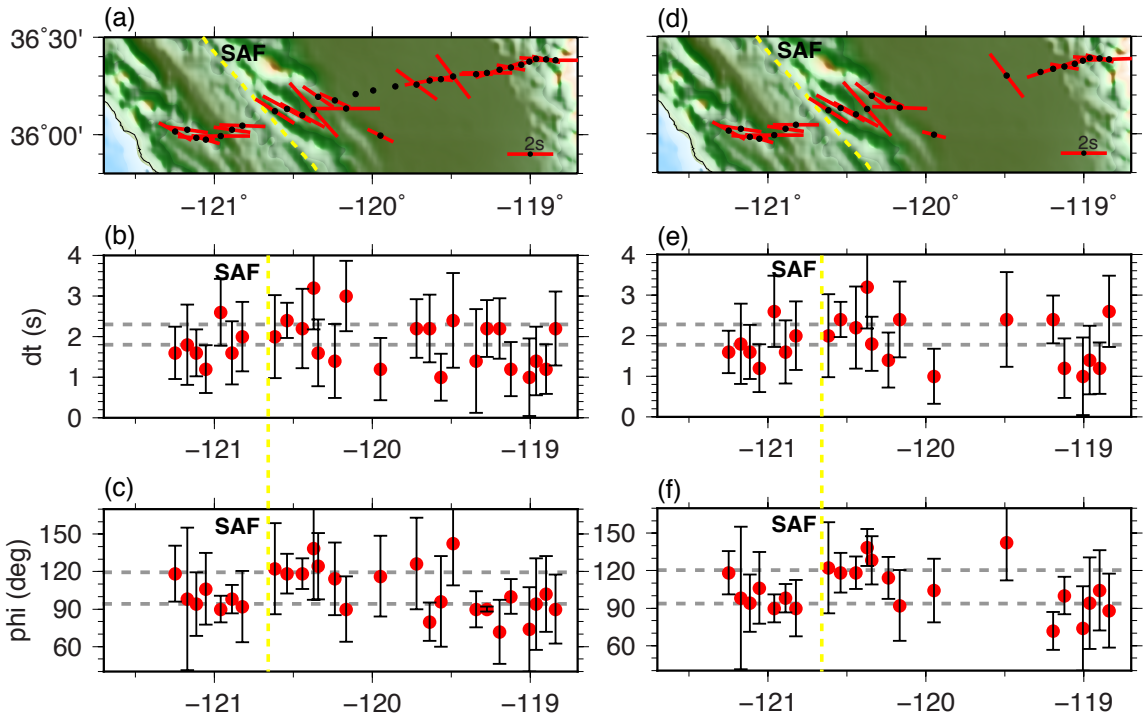

Figure S4. Comparison of single-station average splitting results from using a different culling threshold of SNR with the same criteria of 10° when defining null measurements in the quality control. The left column is from the culling with a SNR of 2, and the right column is with a SNR of 2.5. The first panel shows the geographic distribution of splitting parameters across the CCSE array; the mid panel shows the delay time variations along with the 1-sigma uncertainty from the splitting analysis; the lower panel shows the fast direction variations with the 1-sigma uncertainty. Note that the uncertainties are calculated based on the good non-null measurements at each station.

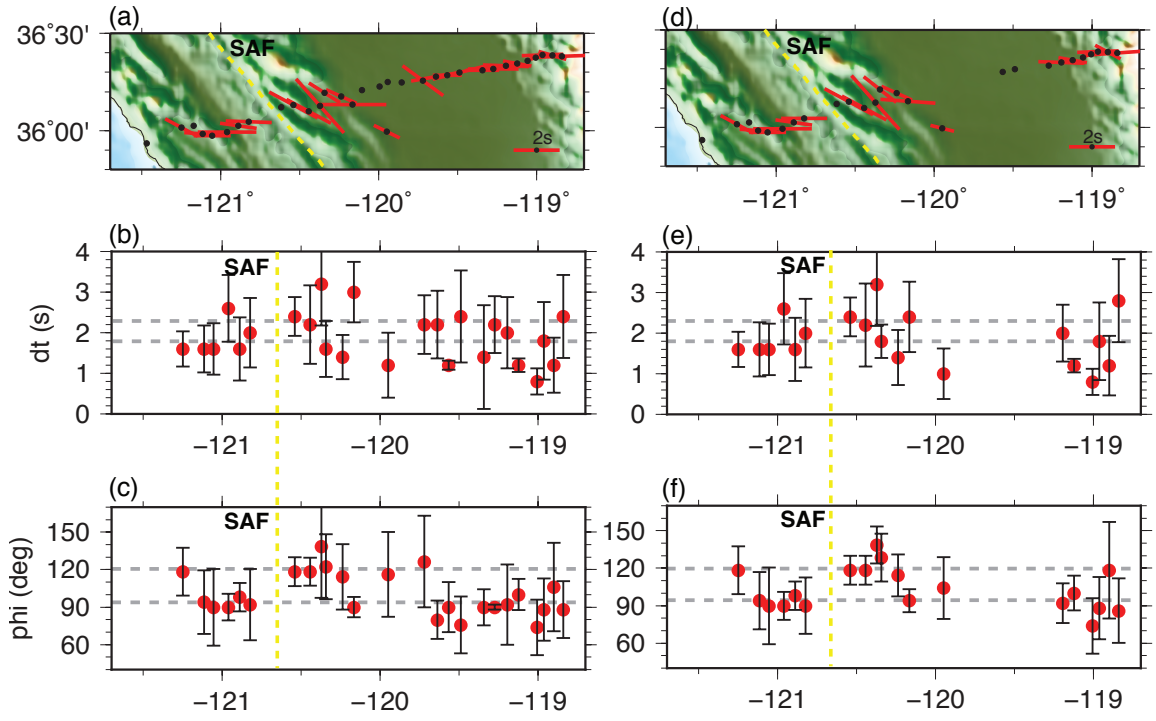

Figure S5. Similar comparison as Fig. S4 of single-station average splitting results from using a different culling threshold of SNR but with the same criteria of 15° when defining null measurements in the quality control. The left column is from the culling with a SNR of 2, and the right column is with a SNR of 2.5.

Figure S6

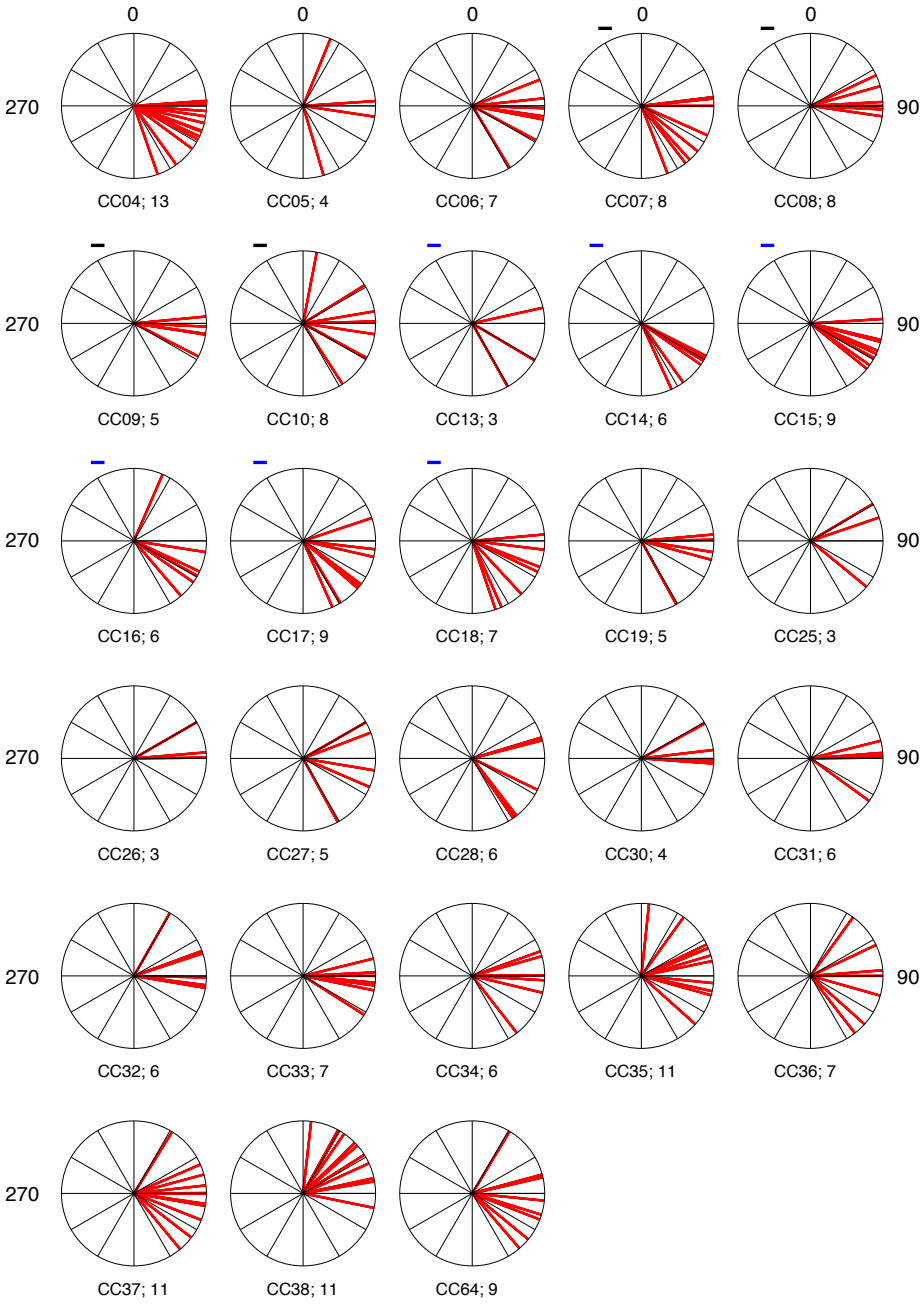

Figure S6. Fast polarization directions of good non-null measurements for each non-null station (with a selection criteria same to that for Fig. 3b) shown as red vectors on a unit circle. The station name and the number of measurements are labeled beneath each diagram. Note that the stations from the two colored circles in Fig. 3a of the main text are illustrated with a colored short bar on the top left of the diagram.

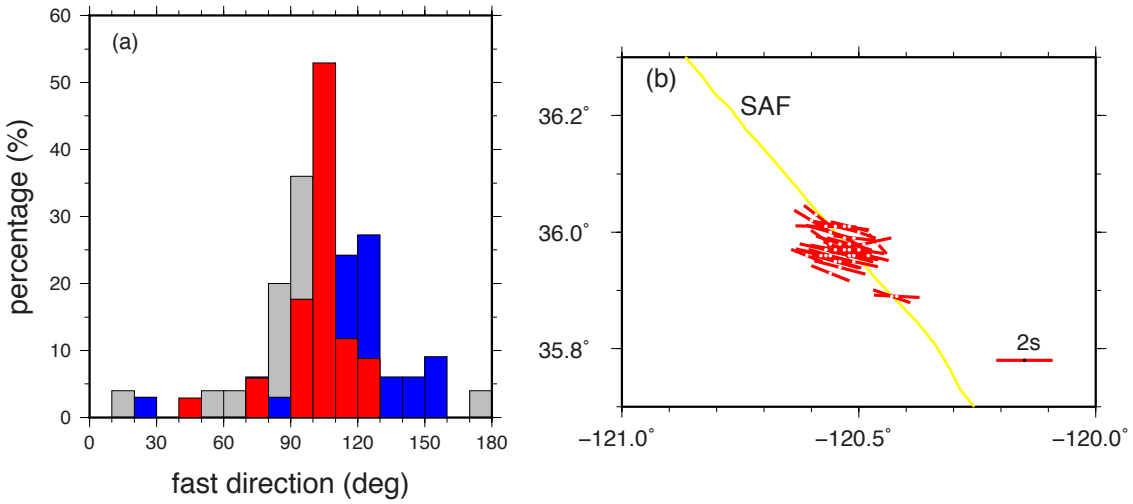

Figure S7. (a) Comparison of the splitting fast direction at SAFOD sites (red column) from Becker et al., (2012) with those from ~35 km west (grey column) and east (blue column) of the SAF from this study. (b) A zoomed-in plot of the splitting measurements at SAFOD sites.

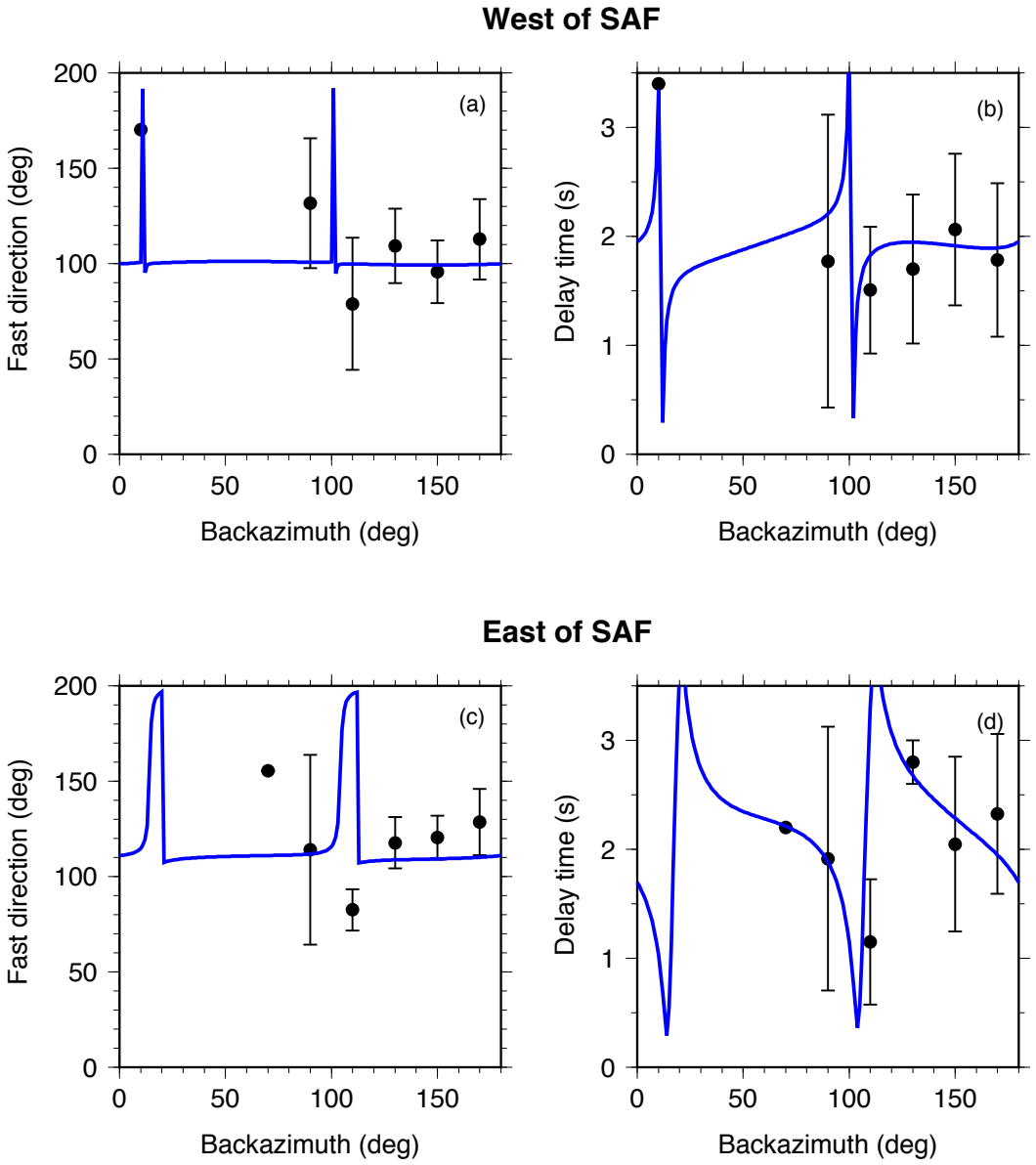

Figure S8. Synthetic splitting results for modelling observed azimuth-dependent splitting behaviors for stations located within 30 km on both sides of the SAF. The forward calculation is conducted using a simple two anisotropic layers with a detailed explanation of model parameters in section 4.2 of the text. The black dots indicate the splitting parameter averaged for all stations within each 20° back-azimuth bin (modulo 180°), and the error bars represent the two standard deviations of all measurements within each bin. Note that the dot at 70° back-azimuth has no error bar due to the lack of good events within that back-azimuth range.

Variable	Definition
SNR of waveforms	The sum of RMS of the noise window (~70 s ahead of the signal window) for the raw Q and T components over the sum of RMS of the signal window for the raw Q and T components
T/Q of the initial waveform	The maximum amplitude of the signal window on raw T component over the maximum amplitude of the same window on raw Q component
T/Q of the corrected waveforms	The maximum amplitude of the signal window on corrected T component over the maximum amplitude of the same window on corrected Q component

Table S1. Definitions of the parameter used for quality control in section 2.

station	longitude	latitude	phi (deg)	1-sigma	dt (s)	1-sigma
CC04	-121.25	36.016	118.31	22.39	1.6	0.65
CC05	-121.172	36.025	98.09	57.12	1.8	0.98
CC06	-121.115	35.984	94.04	25.35	1.6	0.57
CC07	-121.054	35.975	106.18	28.74	1.2	0.59
CC08	-120.961	35.992	90	10.59	2.6	0.82
CC09	-120.889	36.025	98.09	11.35	1.6	0.78
CC10	-120.824	36.046	92.02	28.52	2	0.85
CC13	-120.618	36.121	122.36	36.57	2	1.03
CC14	-120.539	36.131	118.31	15.96	2.4	0.44
CC15	-120.443	36.099	118.31	12.29	2.2	0.97
CC16	-120.371	36.127	138.54	41.14	3.2	1.03
CC17	-120.343	36.194	124.38	26.56	1.6	0.82
CC18	-120.238	36.177	114.27	29.12	1.4	0.91
CC19	-120.165	36.135	90	26.07	3	0.86
CC20	-120.105	36.21	0	0	0	0
CC21	-119.995	36.227	0	0	0	0
CC23	-119.855	36.249	0	0	0	0
CC25	-119.72	36.258	126.4	36.7	2.2	0.72
CC26	-119.637	36.279	79.89	15.31	2.2	0.83
CC27	-119.566	36.286	96.07	36.21	1	0.58
CC28	-119.489	36.298	142.58	33.54	2.4	1.16
CC30	-119.342	36.31	90	14.43	1.4	1.28
CC31	-119.274	36.318	90	2.02	2.2	0.7
CC32	-119.193	36.333	71.8	25.77	2.2	0.75
CC33	-119.122	36.344	100.11	13.8	1.2	0.67
CC34	-119.058	36.36	0	0	0	0
CC35	-119.006	36.376	73.82	33.8	1	0.96
CC36	-118.962	36.389	94.04	36.75	1.4	0.85
CC37	-118.9	36.388	102.13	30.3	1.2	0.61
CC38	-118.841	36.382	90	27.62	2.2	0.91
CWC	-118.08	36.44	102.13	28.76	1.4	0.53
HAST	-121.551	36.389	106.18	29.08	2	0.48
HELL	-119.023	36.68	77.87	24.61	1.2	0.57
ISA	-118.474	35.663	71.8	23.01	1.8	0.57
RAMR	-120.87	35.636	114.27	11.72	1.2	0.72
SMM	-119.996	35.314	112.25	34.54	1	0.64
TIN	-118.23	37.054	67.75	15.39	1.8	0.44

Table S2. Summary of the stacked SKS/SKKS splitting measurements along CCSE array as well as for 7 long-term regional stations used to test the consistency of our analysis with prior results. Note that the stations with 0 value of fast direction and delay time are regarded as null stations (defined in section 3).